J. Fluid Mech. (1969), *vol.* 37, *part* 4, *pp.* 671–688
Printed in Great Britain

A numerical solution of axisymmetric cavity flows

By CHRISTOPHER BRENNEN†
Ship Division, National Physical Laboratory

(Received 29 December 1967 and in revised form 12 December 1968)

In the first part of the paper a method is developed for the relaxation or numerical solution of axisymmetric fully cavitating flows. Employing the technique suggested in a paper by Woods (1951*a*) of working in a transformed (ϕ, ψ)-plane, solutions are obtained for cavities behind a disk and a sphere in different sizes of solid wall tunnel. Under certain conditions flow 'choking' occurs.

The results of a series of experiments carried out with such headforms are then reported. The apparent viscous effect on the position of separation from the sphere and thus on the drag proves to be of particular interest.

1. Introduction

The principal object of this paper is to compare and contrast the axisymmetric potential flow solutions for the steady, fully developed cavity flow past a disk and a sphere with experimental observation. However, the apparent effects of viscosity, surface tension, etc., in these particular cases may be indicative of the influences these properties have in other types of fully developed cavity flow. For the sphere, special interest centres on the comparison of the observed separation position with that calculated using the 'smooth separation' condition (Armstrong 1953).

Numerical or relaxation solutions of the axisymmetric potential flows are obtained in a transformed (ϕ, ψ)-plane, the method being based on the work of Woods (1951*a*). However, the treatment of the cavity surface free streamline is novel. Southwell & Vaisey (1946) obtained relaxation solutions of some free-streamline problems with axial symmetry by working in the physical plane. This necessarily involved 'irregular stars' and the adjustments to the free boundary would seem to have been based on physical reasoning at each stage of the desk calculations. The only cavity solution obtained was of the physically improbable, 'cusped' type.

Of the integral methods employed only the vortex sheet solutions of Armstrong & Dunham (1953) can take into account the separation singularity. Solutions of the flow of an infinite stream past a disk (the separation point therefore being initially known) were obtained by this method. The same problem was also treated by Garabedian (1955) who approached the axisymmetric case by successive corrections to the corresponding planar flow, each correction involving the solution of a linear mixed boundary-value problem. Finally, a number of

---

† Present address: California Institute of Technology, Pasadena.

simple, semi-empirical correspondence methods have been suggested which yield approximate pressure distributions on the axisymmetric wetted surface knowing the distribution for the equivalent planar flow (Fisher 1944; Armstrong & Tadman 1954; Plesset & Shaffer 1948).

2. Mathematical model of the cavity flow

Two particular regions of the cavity flow pose special problems in the setting up of a mathematical, potential flow model and both have received considerable attention in the past. In practice the downstream closure region is marked by considerable turbulence and some local unsteadiness so that no potential flow solution can expect to be accurate in this region. Being the simplest and most widely used, the model of Riabouchinsky (1920), which assumes longitudinal symmetry about a plane through the points of maximum diameter of the cavity, has been employed here. Most authors (e.g. Woods 1961) agree that, within limits, the choice of closure model has little effect on the flow at the upstream end of the cavity and this is confirmed by the results of the present investigation.

The second point is that in real flows separation is essentially a viscous phenomenon occurring where the wetted surface shear stress becomes zero. When the flow is considered as potential and non-viscous and separation takes place from a smooth headform surface it transpires (Woods 1961; Armstrong 1953) that the only 'physically realistic' solution in either planar or axisymmetric flow is given when the radius of curvature of the free streamline is continuous with that of the headform. However, this solution is only 'physically realistic' in the sense that the free streamline neither cuts into the headform nor does it have a concave curvature viewed from the fluid (Birkhoff & Zarantonello 1957). There is of course another class of headform for which the position of separation is fixed by a sharp corner on the body. In this paper solutions are obtained for one headform of each type, respectively a sphere and a disk.

The fact that a relaxation solution is to be obtained imposes the additional condition that the field of flow to be solved must be finite in extent. Thus an upstream boundary, *AF*, and a stream-limiting boundary, *AB*, have been included in the model of the physical plane (figure 1). It is convenient to consider *AB* as a tunnel wall and approach the infinite stream solution asymptotically. By assuming uniform flow or some small deviation from it on the boundary *AF* (see § 5 (i)) the required solution could be obtained by increasing x_U until further increase had a negligible effect on the results.

Stokes's stream function, ψ, and the velocity potential, ϕ, are defined through

$$\frac{\partial \phi}{\partial x} = u = \frac{1}{r}\frac{\partial \psi}{\partial r}, \quad \frac{\partial \phi}{\partial r} = v = -\frac{1}{r}\frac{\partial \psi}{\partial x}, \tag{1}$$

(u, v) being the components in the (x, r)-directions of the velocity vector, q, whose direction is at an angle θ to the axis, $r = 0$. It is convenient to define dimensionless variables as follows:

$$r' = \frac{r}{H}, \quad x' = \frac{x}{H}, \quad q' = \frac{2q}{U}, \quad \Psi = \frac{\psi}{\psi_H}, \quad \Phi = \frac{\phi}{\phi_s}, \tag{2}$$

where U is the uniform upstream velocity, ϕ_s the potential difference between the points E and D and ψ_H the value of ψ on the solid boundary AB. Then equations (1) become:

$$\frac{1}{\alpha}\frac{\partial \Phi}{\partial x'} = u' = \frac{1}{r'}\frac{\partial \Psi}{\partial r'}, \quad \frac{1}{\alpha}\frac{\partial \Phi}{\partial r'} = v' = -\frac{1}{r'}\frac{\partial \Psi}{\partial x'}, \qquad (3)$$

where $\alpha = \tfrac{1}{2}UH/\phi_s$ or $\psi_H/\phi_s H$ since $\psi_H = \tfrac{1}{2}H^2U$.

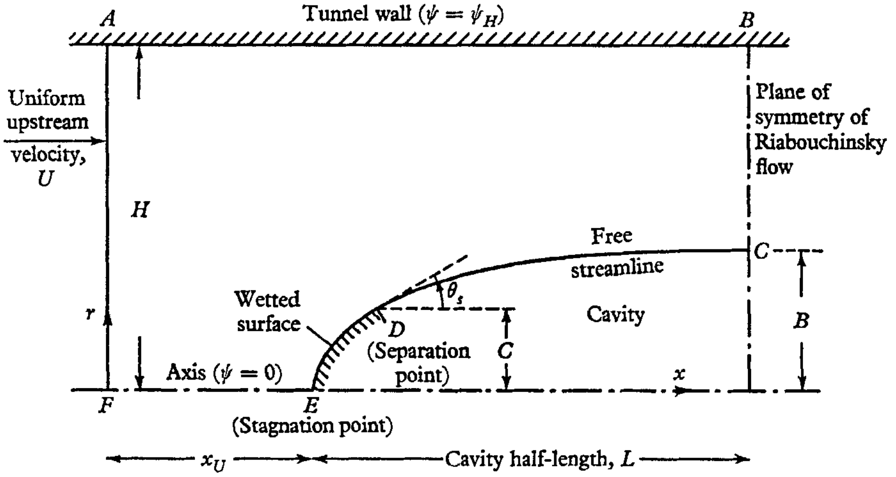

Figure 1. The physical (x, r)-plane.

In the physical plane the positions of the boundaries BC and CD as well as the shape of the latter are initially unknown. In such a problem it is particularly convenient to follow the method of Woods (1951*a*) and, instead of solving for ϕ or ψ in the physical plane, to seek a solution for either x or r in the transformed plane, the dimensionless form of which is shown in figure 2.

For a given headform shape, two parameters define a unique solution in the physical plane: (i) the cavitation number, $\sigma = (p_U - p_c)/\tfrac{1}{2}\rho U^2$, where p_U, p_c are the remote upstream and cavity pressures and ρ is the density of the fluid. Assuming uniform cavity pressure, this specifies the constant free-streamline velocity, $q_c = U\sqrt{(1+\sigma)}$; (ii) the 'blockage ratio', C/H.

The cavitation number must be retained as a solution parameter in the (Φ, Ψ)-plane, defining as it does the boundary condition on CD. But the choice of the dimensionless variables, (2), clearly requires that α replace C/H as the second parameter. The latter will then emerge in the solution of the problem.

Having specified σ and α a unique solution should then be obtainable in the (Φ, Ψ)-plane. Clearly the distance Φ_U is treated in the same manner as would be x_U, being increased until further increase has negligible effect on the results. Thus the geometry of figure 2 is defined except for the distance Φ_F or, in other words, the position of the equipotential boundary BC. This is initially unknown.

The next five sections outline the equations and numerical techniques employed to effect solution.

3. Equations of flow

The equations of Woods (1951*a*) are rewritten in terms of the dimensionless variables, (2), and with the intention of solving for $g = (r')^2$ in the (Φ, Ψ)-plane:

$$\alpha\frac{\partial x'}{\partial\Phi} = \frac{u'}{q'^2} = \frac{1}{2}\frac{\partial g}{\partial\Psi}, \quad \frac{\alpha}{2g^{\frac{1}{2}}}\frac{\partial g}{\partial\Phi} = \frac{v'}{q'^2} = -g^{\frac{1}{2}}\frac{\partial x'}{\partial\Psi}. \tag{4), (5}$$

The field equation governing g becomes

$$\alpha^2\frac{\partial^2 \ln g}{\partial\Phi^2} + \frac{\partial^2 g}{\partial\Psi^2} = 0. \tag{6}$$

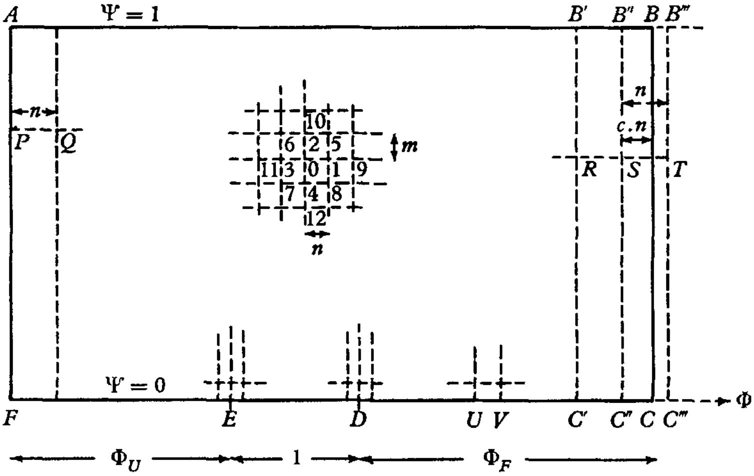

FIGURE 2. The dimensionless (Φ, Ψ)-plane.

From the solution, $g(\Phi, \Psi)$, the values of u', v', q', θ and x' at any point can be obtained by employing (4) and (5) and relations which follow from those expressions:

$$\frac{4}{q'^2} = \frac{\alpha^2}{g}\left(\frac{\partial g}{\partial\Phi}\right)^2 + \left(\frac{\partial g}{\partial\Psi}\right)^2, \quad \tan\theta = \alpha\frac{\partial g}{\partial\Phi}\bigg/ g^{\frac{1}{2}}\frac{\partial g}{\partial\Psi}, \tag{7), (8}$$

$$dx' = \frac{1}{2\alpha}\frac{\partial g}{\partial\Psi}d\Phi - \frac{\alpha}{2g}\frac{\partial g}{\partial\Phi}d\Psi. \tag{9}$$

4. Numerical and relaxation equations

To effect the numerical solution, the (Φ, Ψ)-plane was first covered by a mesh or net, parts of which are shown in figure 2. The net included the boundaries *AB*, *CDEF* and *AF* as mesh lines and the points *A*, *D*, *E* and *F* as nodes. The initially unknown position of *BC* was defined, relative to the particular mesh lines $B''C''$ and $B'''C'''$ by the fractional mesh length, $c.n$ (figure 2), c eventually being determined as part of the solution. Conventional finite-difference methods yield the following approximation to the field equation, (6), at a general node 0 (the points surrounding that node being labelled as indicated in the middle of figure 2):

$$\left(\frac{\alpha m}{n}\right)^2 \ln\left(\frac{g_1 g_3}{g_0^2}\right) + g_2 + g_4 - 2g_0 = 0 \quad (= Y_0), \tag{10}$$

where the mesh intervals in Φ and Ψ are n and m. The intrinsic error is a function of m^4, n^4, $\partial^4 \ln g/\partial\Phi^4$, $\partial^4 g/\partial\Psi^4$ and higher orders and powers. This equation being non-linear, a point-by-point Gauss–Seidel iterative procedure, starting with 'guessed' values of g at all nodes, was employed for solution. Superscripts, i, denoting the value at a node after i iterations, this involved repeating the following operation at every point:

$$g_0^{i+1} = g_0^i + \omega(-Y_0)^i \Big/ \left[\frac{\partial Y_0}{\partial g_0}\right]^i, \tag{11}$$

where Y_0 is the residual or particular value of the left-hand side of (10) during that moment in the iterative process and ω is a chosen over-relaxation factor.

5. Boundary conditions

The boundary conditions and their finite-difference forms must be briefly listed. (i) On the upstream boundary, AF, the simplest condition would be to assume uniform flow, $g = \Psi$. However, an improvement upon this reduced the minimum Φ_U necessary for satisfactory solution. A study of the various analytic solutions for axisymmetric non-separating flows past simple bodies (Lamb 1932) revealed that for two points such as P and Q (figure 2) the relation

$$\frac{g_Q - \Psi_P}{g_P - \Psi_P} = \left[\frac{\Phi_U^2 + 4\alpha^2\Psi_P}{(\Phi_U - n)^2 + 4\alpha^2\Psi_P}\right]^{\frac{3}{2}} \tag{12}$$

was an accurate solution to the upstream flow provided $(g_Q - \Psi_P) \ll \Psi_P$. This alternative boundary condition, already in numerical form since it relates g_P to g_Q, allows some perturbation from uniform flow. It remains to note that the use of this condition means that the equipotential, AF, no longer necessarily transforms back into a line of constant x in the physical plane. (ii) On the wall, AB, $g = 1$ and on the axis, EF, $g = 0$. (iii) On the wetted surface boundary, DE, the function $\theta(g)$ is known for a particular headform. Thus, through (8), the conditions on DE for the disk and sphere become respectively

$$\frac{\partial g}{\partial \Psi} = 0 \quad \text{and} \quad \frac{\partial g}{\partial \Phi} = \left[\frac{g_D}{\cos^2\theta_s} - g\right]^{\frac{1}{2}} \frac{\partial g}{\partial \Psi}, \tag{13}$$

where g_D is the value of g and θ_s the angle of flow at the separation point, D. Neither of these quantities is initially known and their 'relaxation' is discussed in the next section. The physical radius of the sphere is determined from the solution by the relation $(R/H)^2 = g_D/\cos^2\theta_s$. Finite-difference forms of the first derivatives, inserted in (13) complete the governing equations for node points, O, on DE.

$$\left(\frac{\partial g}{\partial \Psi}\right)_0 \approx \frac{1}{6m}\left[8g_2 - g_{10} - 7g_0 + 2\left(\frac{\alpha m}{n}\right)^2 \ln\left(\frac{g_1 g_3}{g_0^2}\right)\right], \tag{14}$$

$$\left(\frac{\partial g}{\partial \Phi}\right)_0 \approx \frac{1}{6n}[6g_1 - g_9 - 2g_3 - 3g_0] \quad \text{or} \quad \frac{1}{6n}[-6g_3 + g_{11} + 2g_1 + 3g_0]. \tag{15}$$

These contain the same order of error as the field equation, (10). (iv) The condition of symmetry about the boundary, BC, leads to the following relation for the value of g at a point such as T (figure 2) in terms of the values at R and S:

$$(2c+1)\,g_T = 4cg_S + (1-2c)\,g_R. \tag{16}$$

A value for c is obtained for each iteration by the method outlined below. (v) The requirement of constant velocity on the free streamline leads, through (7), to the following condition on DC:

$$\sigma = \left[\frac{\alpha^2}{g_0}\left(\frac{\partial g}{\partial \Phi}\right)^2 + \left(\frac{\partial g}{\partial \Psi}\right)^2\right]^{-1} - 1, \tag{17}$$

where the expressions (14) and (15) were again used for the first derivatives. The value of the right-hand side at a particular moment in the iterative process is termed the 'local cavitation number', σ_0, and it is convenient to consider $(\sigma_0 - \sigma)$ as the residual at a general point, O, on the boundary DC. Now if the procedure of (11) were followed the residual at a boundary point such as U (figure 2) would be dispersed by changing g_U. It can be shown that this would almost invariably imply that g_U ought to be decreased if σ_U were greater than σ. But this is contrary to physical experience; as the size of a cavity increases, σ decreases. On the other hand, if the residual at U were dispersed by altering g_V rather than g_U then the numerical equations indicate a direction of change compatible with physical experience. Further, this second mode of relaxation on the boundary EF, unlike the first suggested method, provides a means of computing a new value for the fractional mesh length, c, after each iteration. The most downstream point at which $(\sigma_0 - \sigma)$ can be computed is C'' (figure 2). Use of the second method then determines a new value at C''' and substituting $g_{C'}, g_{C''}, g_{C'''}$ into (16) yields a new value of c which can then be used universally to determine values at all other points on $B'''C'''$. Essentially, this procedure amounts to convecting the residuals on DC downstream and finally eliminating them by adjusting the position of the boundary BC.

The actual procedure adopted differed only in detail from this second method. Care had to be taken to achieve satisfactory convergence. Thus it was found desirable to define the g values on EF by the recurrence relation, $d_0 = g_1 - g_0$, and to use the slightly modified procedure

$$d_0^{i+1} = d_0^i - \frac{\beta_1(\sigma_0^i - \sigma)}{[\partial\sigma_0/\partial g_1]^i},$$

β_1 being a chosen constant. Further experience indicated that stability and convergence were enhanced by simplifying this to

$$d_0^{i+1} = d_0^i - n\beta_2(\sigma_0^i - \sigma),$$

where the factor β_2 was suitably optimized.

6. Singularities

Special treatments had to be devised for the groups of nodes in close proximity to the singular points at stagnation and separation, since the larger values of the higher derivatives in these regions lead to unacceptably large errors in the normal finite-difference approximations. Owing to the non-linearity of the governing equation (6) the 'function splitting' methods of Russell (1963), Woods (1951*b*) and others are unfortunately not available. However, satisfactory results were obtained by imposing upon those groups of points an analytic solution known to be of the correct type and containing a number of initially unknown constants by which it could be matched into the surrounding finite-difference solution. Initial computations determined the minimum necessary size of the region to be treated.

For this purpose, the analytic solutions for the non-separating flow past a disk and a sphere (Lamb 1932) were employed in the vicinity of the respective stagnation points. Since, for example, the flow near the disk stagnation point in the cavitating solution could probably be better matched by the non-cavitating analytic solution for a disk of different radius, the 'headform size' in both analytic solutions was employed as a matching constant.

In the case of separation, however, analytic solutions had to be developed from scratch for use near that singularity. A modified set of co-ordinates, (ξ, η), with origin at the separation point, D, were defined so that

$$\xi = \frac{1}{2\alpha(1+\sigma)^{\frac{1}{2}}}\frac{\Phi}{g_D^{\frac{1}{2}}}, \quad \eta = \frac{1}{2(1+\sigma)^{\frac{1}{2}}}\frac{\Psi}{g_D},$$

and the corresponding polar co-ordinates denoted by (ρ, τ), where $\tau = 0$ described the free streamline, $\tau = \pi$ the wetted surface. Then it was assumed that the solution close to the origin could be written in the form

$$\frac{g}{g_D} = h = 1 + \sum_{k=1}^{\infty} \rho^{t_k} F_k(\tau),$$

where the powers, t_k, and the functions $F_k(\tau)$ were initially unknown. The condition of finite, non-zero flow velocity at separation demanded that $t_1 = 1$. Then substitution into the field equation (6) and the boundary conditions eventually produced the following solution for the case of the disk:

$$h = 1 + [2\cos\tau]\rho + [K_1 \sin(3\tau/2)]\rho^{\frac{3}{2}} + \left[1 - \frac{9K_1^2}{32}\cos 2\tau\right]\rho^2 + \ldots, \tag{18}$$

K_1 being an arbitrary constant. Further algebra revealed that a positive, non-zero K_1 implied that the radius of curvature of the free streamline (positive if convex viewed from the fluid) tended to $+\infty$ and the pressure gradient on the wetted surface to $-\infty$ as the separation point was approached. Armstrong (1953) termed this 'abrupt' separation since it can clearly only occur from a sharp edge on the headform.

A similar expression was obtained for the sphere. However the only 'physically realistic' case (see § 2) is that for which the constant corresponding to K_1 is zero, yielding the 'smooth separation' solution:

$$h = 1 + [2\cos\theta_s \sin\tau + 2\sin\theta_s \cos\tau]\rho$$
$$+ [\sin\theta_s \cos\theta_s \sin 2\tau - \cos^2\theta_s \cos 2\tau + \sin^2\theta_s]\rho^2 + \ldots \quad (19)$$

Truncating (18) and (19) at the same power (ρ^2) produced analytic solutions with two matching constants in each case; g_D and K_1 for the disk, g_D and θ_s for the sphere. In this way the angle of separation from the sphere emerged from the solution. In addition, these relations provided the values of g at the first few nodes on DC thus initiating the free-streamline relaxation procedure described in § 5.

7. Further remarks. The phenomenon of choked flow

Though the essential points of the numerical method of solution are contained in the preceding sections, much of the detail has been omitted, having been reported elsewhere (Brennen 1966). Test solutions, error and convergence analyses were employed in determining the most efficient mesh geometry; the final net contained much smaller m, n in the region of the wetted surface than, say, near the tunnel wall. Error analyses of the solutions reported upon here indicated a maximum possible error in the g values of less than 0·5 %. Stability restrictions on the over-relaxation factors limited convergence. Typically one solution required 30 min on a KDF 9 computer.

Finally it remains to note that, for a certain range of the parameters α and σ, solutions of the present type are unobtainable. Cavity flows in streams limited by solid walls exhibit a phenomenon in which, for a given stream and cavity pressure, the velocity of the flow cannot be increased above a certain maximum. This limit, termed 'choked flow', was investigated by Birkhoff, Plesset & Simmons (1950) for the case of planar flow. It can be shown (Birkhoff & Zarantonello 1957) that the following simple relations hold for choked axisymmetric flows of the type given by figure 1.

$$(B/H)_{\text{choked flow}} = [1 - (1+\sigma)^{-\frac{1}{2}}]^{\frac{1}{2}}, \quad (20)$$

$$(C_D)_{\text{choked flow}} = (H/C)^2\,[(1+\sigma)^{\frac{1}{2}} - 1]^2, \quad (21)$$

C_D being the coefficient of drag $[C_D = (\text{drag})/\frac{1}{2}\pi\rho U^2C^2)]$. In this limit the cavity is infinitely long. Thus the condition is independent of the choice of cavity closure model. It can also be shown that, for a given σ, the minimum values of both C_D and (C/B) occur at choking. In non-choked flows the right-hand sides of (20) and (21) are denoted by (B^*/H) and C_D^*. Thus, for example, the intersections of curves for C_D and C_D^* against H/C for fixed σ locate the choked condition.

8. Experiments

In a series of experiments, carried out in the no. 2 water tunnel of Ship Division, N.P.L. (Silverleaf 1960), natural cavities behind 3 in. and $1\frac{1}{8}$ in. diameter spherical and 3 in. diameter diskal headforms were produced and photographed with high-speed flash equipment (exposure $\sim 20\mu$s). The headforms were supported with their centres on the axis of the 44 in. diameter working section by means of a downstream sting itself supported by a radial strut (Brennen 1969). At a particular tunnel velocity, U (up to 45 ft./s), different σ were obtained by varying the tunnel pressure, p_U (minimum about 2·4 in.Hg). For the larger sphere and the disk, σ, was computed from mercury vacuum manometer measurements of the cavity pressure, p_c. The pressure line to a tapping in the back face of the headform was cleared of any possible water drop blockage by a short burst of air prior to each reading (as recommended by Gadd & Grant 1965). Details of these measurements and their relation to the water vapour pressure, p_v, are given elsewhere (Brennen 1969). The values of σ for the $1\frac{1}{8}$ in. sphere are less accurate, being based on the assumption $p_c = p_v$, though the air content of the water was maintained at a low value ($\sim$ 4 p.p.m.) to minimize the error.

The distances from the front stagnation point to the rear closure point (L_1) of cavities behind the 3 in. sphere were measured from a scale attached to the tunnel window. The positions of separation from the two spheres were estimated from the photographs and, for the larger headform, by using a parallax method employing axes and scales fixed to the windows on opposite sides of the working section. The latter method revealed that the separation position required some minutes to adjust itself after a change in the flow conditions, but thereafter virtually no variation was observed. The results of these experiments are used for comparison in figures 9 and 13, and figures 14 and 15, plates 1 and 2.

9. Results for the disk

The pressure distributions on the wetted surface of the disk for given σ, different H/C were indistinguishable on the scale of figure 3. Variation with σ was also small and only the distributions for $\sigma = 0{\cdot}3$ and 0·7 are shown since the curves for other σ lay regularly in relation to these. There is close agreement with the experimental measurements of Rouse & McNown (1948) of which those for $\sigma = 0{\cdot}24$ are shown. The results for C_D, presented in figure 4, exhibit a total variation in $C_D/(1+\sigma)$ of under $2\frac{1}{2}$ %, clearly demonstrating the accuracy of Reichardt's (1945) empirical formula, which treats it as constant. On the scale of figure 4, the corresponding graphs of $C_D^*/(1+\sigma)$ deviate negligibly from the verticals indicated. Owing to the evidently small angle of intersection it was not feasible to predict the choked conditions in figure 4. The infinite-stream values are replotted in figure 5 and compare favourably with those of Garabedian (1955) and Armstrong & Dunham (1953). Fisher's (1944) correspondence principle (see § 1) is evidently more accurate than that of Plesset & Shaffer (1948), the curve for the latter lying below the horizontal axis of figure 5. Experimental measurements by Reichardt (1945) and Eisenberg & Pond (1948) yielded values of 0·79

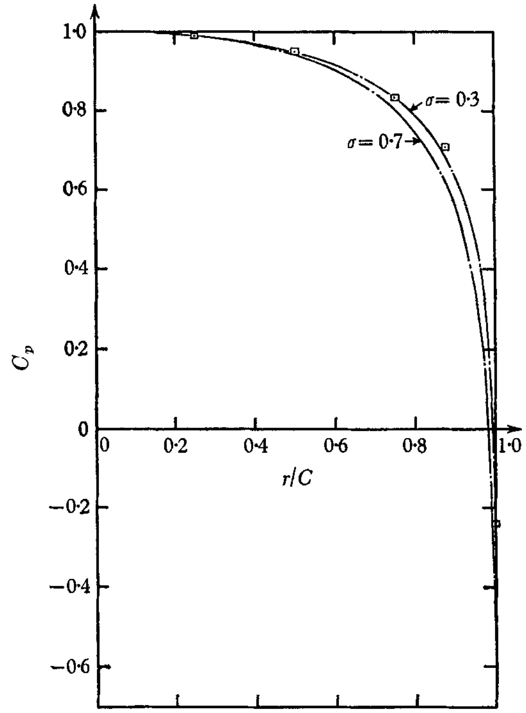

FIGURE 3. Pressure distributions on the surface of the disk. Coefficient of pressure, C_p, is $(p-p_U)/\frac{1}{2}\rho U^2$ or $1-(q/U)^2$. ——·——, Values of C_p computed for $\sigma = 0·3$ and $0·7$; ⊡, experimental measurements for $\sigma = 0·24$ by Rouse & McNown (1948).

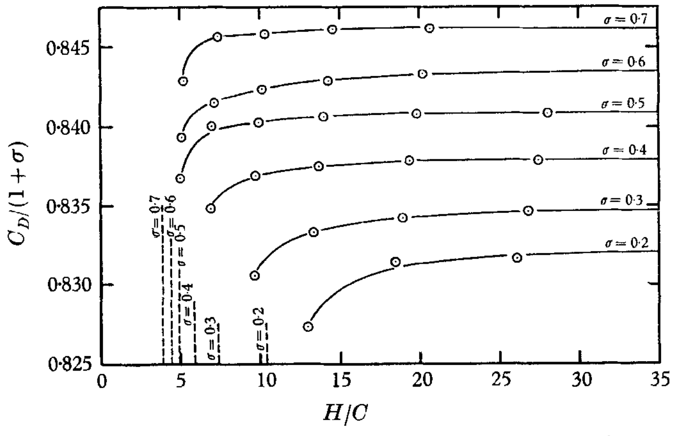

FIGURE 4. Disk results. ——⊙——, $C_D/(1+\sigma)$; - - - - -, $C_D^*/(1+\sigma)$.

and 0·80 respectively, any variation with σ being outside possible experimental accuracy. Significantly lower experimental values of $C_D/(1+\sigma)$ could be due to the assumption of $p_c = p_v$, yielding higher σ than actually pertain since $p_c > p_v$. The impossibility in real flows of the theoretical, infinite pressure gradient at separation may lead to a reduction in the surface pressure just upstream of that point (for a given σ) and thus a lower drag.

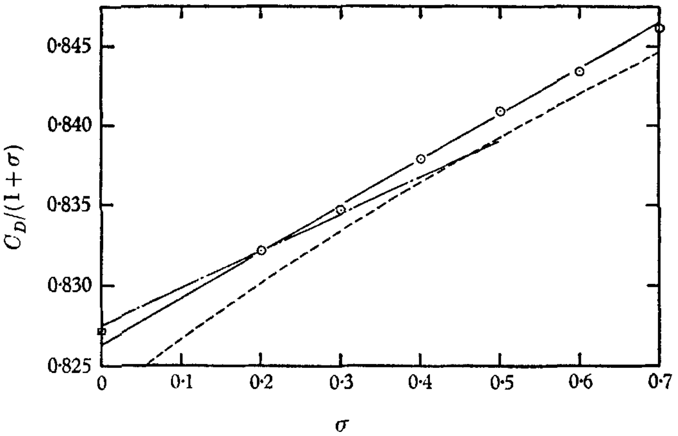

FIGURE 5. Disk results for $H/C = \infty$. — · —, Armstrong & Dunham (1953); - - - - -, Fisher (1944); ☐, Garabedian (1955); —○—, present results for $H/C = \infty$.

In figure 14, the corresponding theoretical cavity profile has been superimposed upon one of the photographs of cavities behind the 3 in. disk. The profiles virtually coincide. In figure 6 the results for $(C/B)^2$ and $(C/B^*)^2$ have been tentatively extrapolated to predict the 'choked flow line'. The construction was aided by assuming that the limiting condition occurred at the values of H/C given by the near-vertical lines in figure 4. The main dimensions of the cavity, $(C/B)^2$ and (C/L), are compared in figures 7 and 8 with the experimental measurements of Rouse & McNown (1948) and Eisenberg & Pond (1948), with the theoretical results of Armstrong & Dunham (1953) and with Reichardt's (1945) empirical formulae though the last was only designed for the range $0 < \sigma < 0{\cdot}1$ from measurements in a free jet tunnel.

10. Results for the sphere

The computed and experimentally observed positions of separation from the spherical headforms are presented in figure 9 ($(90-\theta_s)$ being the angle between stagnation and separation in degrees) along with the measurements of Hsu & Perry (1954). Armstrong & Tadman (1954) employed an approximate similitude relation to obtain their theoretical line (see also figure 11) from that of the corresponding planar flow past a cylinder (also shown). Incidentally, their curves show θ_s tending to zero as $\sigma \to \infty$. But, since the Riabouchinsky model is used, the limiting condition of no cavity must surely be given by the respective fully

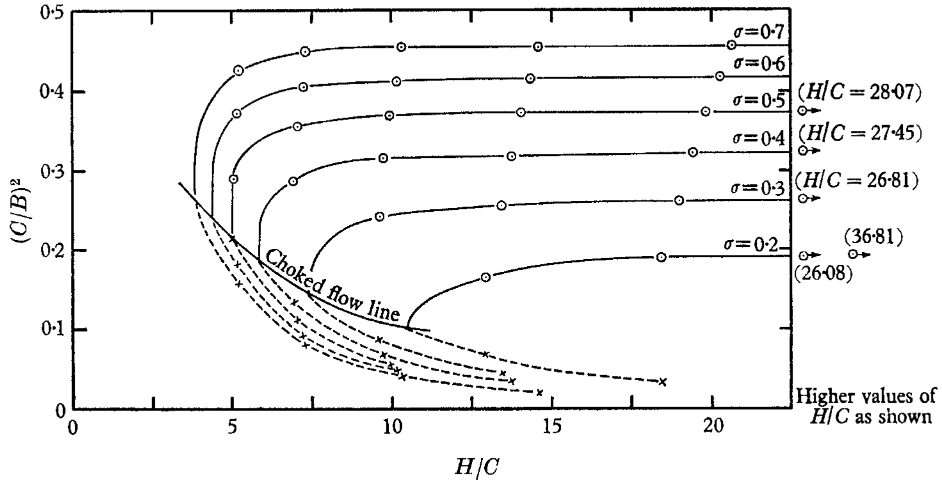

FIGURE 6. Disk cavity width parameter as a function of H/C and σ. —○—, results obtained for $(C/B)^2$; – – – × – – –, corresponding curves for $(C/B^*)^2$.

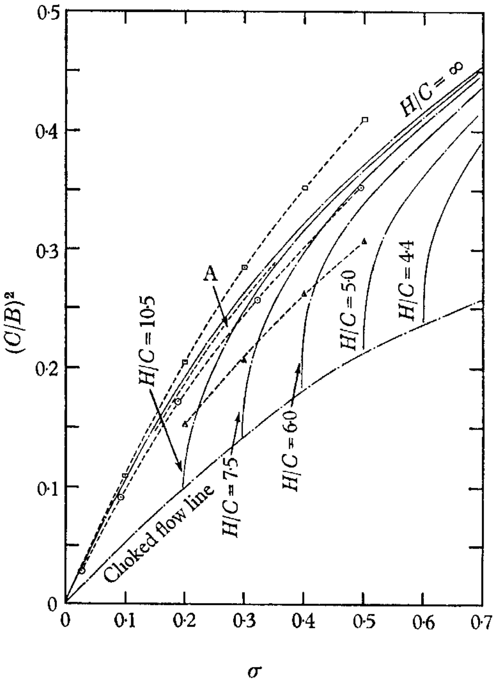

FIGURE 7. Disk cavity width parameter as a function of σ and H/C. —□—, Reichardt's (1945) formula; —○—, Armstrong & Dunham 1953; —△—, Rouse & McNown (1948) A — —, Eisenberg & Pond (a mean line); — · —, present results for various H/C as marked.

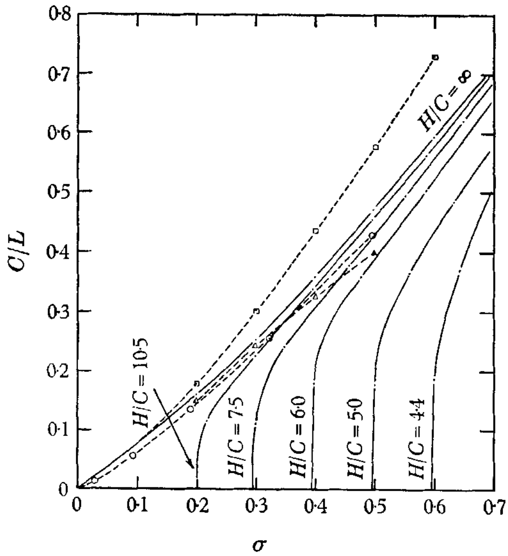

FIGURE 8. Disk cavity half-length parameter as a function of σ and H/C. —□—, Reichardt's (1945) formula; —⊙—, Armstrong & Dunham (1953); —△—, Rouse & McNown (1948); — - —, present results for various H/C as marked.

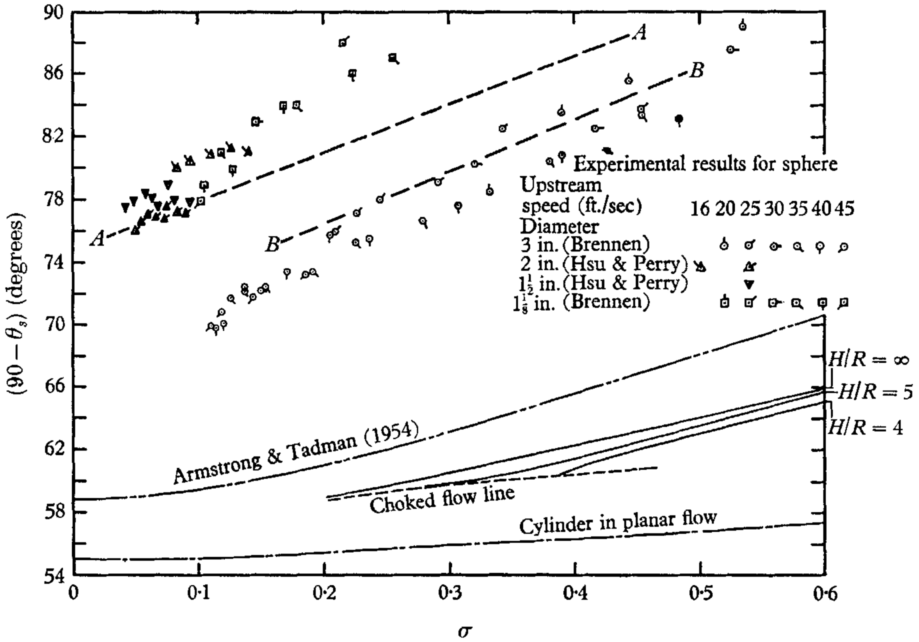

FIGURE 9. Computed and observed locations of separation from the spherical headforms.

attached potential flows; that is to say as $\theta_s \to 0$, $\sigma \to 1\frac{1}{4}$ and $C_D/(1+\sigma) \to \frac{1}{2}$ for the sphere and $\sigma \to 1\frac{1}{2}$, $C_D/(1+\sigma) \to \frac{2}{3}$ for the cylinder.

Examination of the variation in the difference between theoretical and experimental separation positions does seem to reveal a fairly consistent dependence on the Reynolds number, $Re = 2UR/\nu$. Thus the lines *AA* and *BB* may represent the real positions for Reynolds number of $3{\cdot}4 \times 10^5$ and $5{\cdot}2 \times 10^5$ respectively. Since, on the other hand, the scatter does not correlate at all well on the basis of Weber number it must be concluded that the influence of surface tension on the separation position is minor compared with the viscous effect.

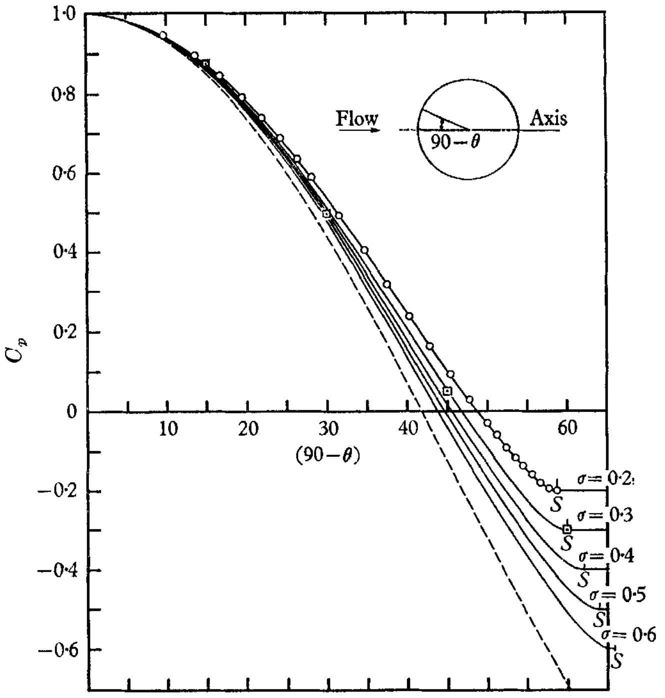

FIGURE 10. Pressure distributions on the wetted surface of the sphere for various σ as shown. — — — —, potential non-cavitating distribution; □, experimental, Rouse & McNown (1948) ($\sigma = 0{\cdot}3$); —$\overset{|}{S}$—, separation points; ——○——, individual mesh point values of C_p (for $\sigma = 0{\cdot}2$).

As in the case of the disk the pressure distributions on the wetted surface of the sphere for a particular σ and different *H*/*C* were indistinguishable on the scale of figure 10 except for the slight change in separation position. The experimental measurements of Rouse & McNown (1948), of which those for $\sigma = 0{\cdot}3$ are shown, again agreed closely with the computed results. The variation in $C_D/(1+\sigma)$ encountered ($\sim 20\,\%$) was, however, much greater than for the disk. Owing to the fact that results were obtained close to the choked condition it was feasible to estimate that limit and plot curves for various *H*/*R* in figure 11. The experimental measurements of drag due to Waid (1957), Eisenberg & Pond (1948) and Hsu & Perry (1954) all lie significantly below the respective theoretical curves in figure 11. This is somewhat surprising since it might be argued that, with the higher experimental values of $(90-\theta_s)$ and pressure distributions similar to those of figure 10, the experimental drag ought to be greater than the theoretical. A clue to the explanation of these apparently anomalous results may, however, lie in the following observation. The experimental pressure distribution measurements of

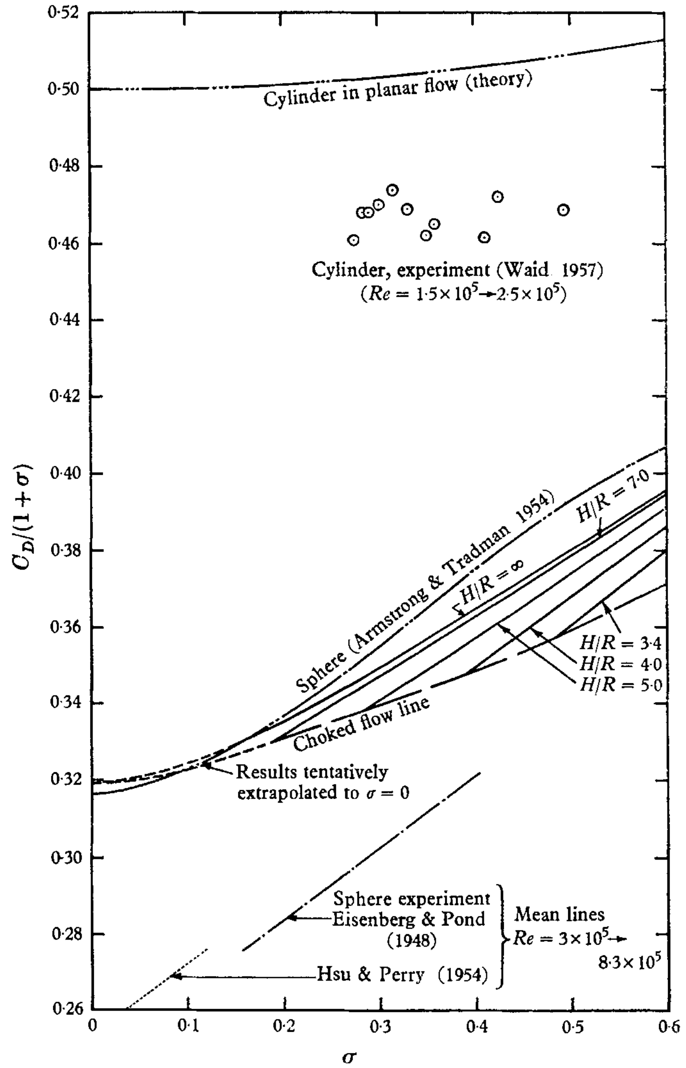

FIGURE 11. Drag parameter as a function of σ.

Rouse & McNown (1948) (1 in. sphere) and Konstantinov (1950) (5–50 mm spheres) for fully developed cavities (roughly $\sigma < 0{\cdot}7$) are not only close to theory but also indicate that cavity pressure is reached at about 60° to 65° from the stagnation point. Thus it appears that there may be a region of attached flow of virtually constant pressure between the theoretically predicted and actual separation points. Since the time required for vaporization is large compared with

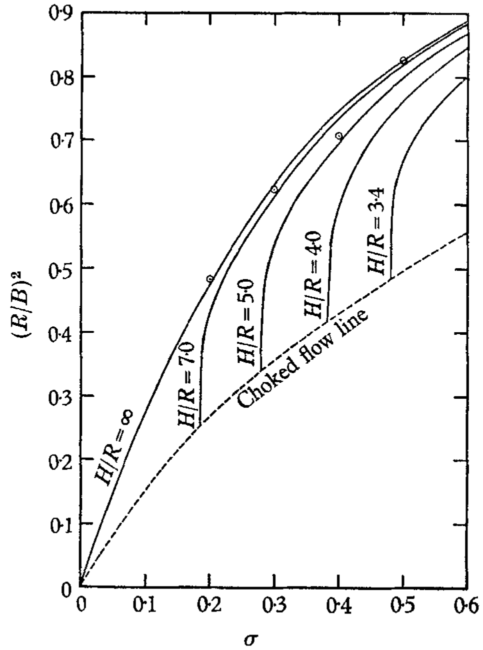

FIGURE 12. Sphere. Maximum cavity radius as a function of σ and H/R. ○, Rouse & McNown (1948), experiment; ———, present results for various H/R; - - - - -, result for choked flow.

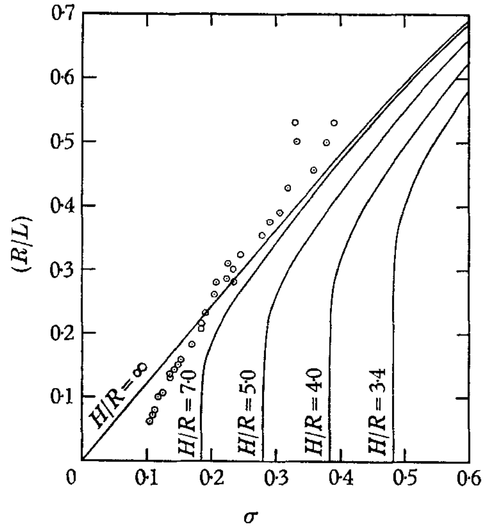

FIGURE 13. Sphere. Cavity half-length parameter as a function of σ and H/R. ○, experimental results ($H/R = 14·67$); ———, present results for various H/R as marked.

the residence time of fluid particles, it seems reasonable to assume that this region includes pressures lower than p_c in order to produce the small but necessary adverse pressure gradient required to effect viscous separation. This may account for some reduction from the theoretical drag. However, low values of $C_D/(1+\sigma)$ may, as mentioned in the last section, also result from underestimating p_c.

In figure 15, the corresponding theoretical cavity profile has been superimposed on one of the photographs taken during the experiments with the 3 in. sphere. Though at this magnification the photographic definition is poor, it would appear that the greatest discrepancy occurs near the actual separation point and that the downstream cavity surface asymptotes roughly to the theoretical. Boundary-layer growth in the roughly constant pressure zone upstream of separation and its dispersion following separation could account for the difference between the two profiles. The angle between the tangents to the cavity surface and the headform at separation (about 7°) is typical in general of boundary-layer separation.

The cavity dimension parameters, $(R/B)^2$ and (R/L), are plotted in figures 12 and 13. In the last figure, the measured values of $(2R/L_1)$ from the 3 in. sphere experiments lie along a curve compatible with theory since the relevant H/R is 14·67. However, as σ is increased and the size of the cavity is reduced, the Riabouchinsky model becomes less accurate and the values for the smallest cavities begin to depart from the theoretical line.

11. Concluding remarks

Comparison with experiment suggests that the solutions obtained by the numerical method are quite accurate. The flow is particularly well modelled in the case of the headform with a fixed separation point, namely the disk. Observed separation from the sphere occurs well downstream of the position predicted by theory, owing principally to boundary layer or viscous effects. Despite and apart from this it would appear that the flow is satisfactorily modelled by the assumption of 'smooth' separation. The present evidence suggests the existence of a region of virtually constant wetted surface pressure between the theoretically predicted and actual separation positions. Detailed pressure measurement in this zone is required to confirm this. Investigations of the variation of pressure and the vapour flow within a cavity and accurate measurement of p_c may account for the measured drag being almost invariably smaller than that predicted by theory.

I should like to express my sincerest gratitude to Dr L. C. Woods under whose supervision the theoretical work was carried out and submitted as a D.Phil. thesis in the University of Oxford. This was financed by a generous grant from the Ministry of Education for Northern Ireland.

The assistance received from Mr S. Grant, Mr D. Swindells and Dr G. E. Gadd, whilst carrying out the experiments at Ship Division, N.P.L., was much appreciated.

REFERENCES

ARMSTRONG, A. H. 1953 Abrupt and smooth separation in plane and asixymmetric flow. *Memor. Arm. Res. Est. G.B.* no. 22/63.

ARMSTRONG, A. H. & DUNHAM, J. H. 1953 Axisymmetric cavity flow. *Rep. Arm. Res. Est. G.B.* no. 12/53.

ARMSTRONG, A. H. & TADMAN, K. G. 1954 Axisymmetric cavity flow about ellipsoids. *Proc. of the Joint Admiralty-U.S. Navy Meeting on Hydroballistics.*

BRENNEN, C. 1966 D.Phil. Thesis, University of Oxford.

BRENNEN, C. 1969 The dynamic balances of dissolved air and heat in natural cavity flows. *J. Fluid Mech.* **37**, 115.

BIRKHOFF, G., PLESSET, M. & SIMMONS, N. 1952 Wall effects in cavity flows, I. *Q. appl. Math.* **8**, 151. Wall effects in cavity flows, II. *Q. appl. Math.* **9**, 413.

BIRKHOFF, G. & ZARANTONELLO, E. H. 1957 *Jets, Wakes and Cavities.* New York: Academic Press.

EISENBERG, P. & POND, H. L. 1948 Water tunnel investigations of steady state cavities. *David Taylor Model Basin Report,* no. 668.

FISHER, J. W. 1944 The drag on a circular plate generating a cavity in water. *Underwater Ballistics Commun.* no. 17.

GADD, G. E. & GRANT, S. 1965 Some experiments on cavities behind disks. *J. Fluid Mech.* **23**, 645.

GARABEDIAN, P. R. 1955 The calculation of axially symmetric cavities and jets. *Pacif. J. Math.* **6**.

HSU, E-Y. & PERRY, B. 1954 Water tunnel experiments on spheres in cavity flow. *Calif. Inst. of Tech. Report,* no. E-24.9.

KONSTANTINOV, V. A. 1950 Influence of Reynolds number on the separation (cavitation) flow. *David Taylor Model Basin Translation,* no. 233.

LAMB, H. 1932 *Hydrodynamics.* Cambridge University Press.

PLESSET, M. S. & SHAFFER, P. A. 1948 Cavity drag in two and three dimensions. *J. appl. Phys.* **19**, 10.

REICHARDT, H. 1945 The physical laws governing the cavitation bubbles produced behind solids of revolution in a fluid flow. *The Kaiser Wilhelm Institute for Hyd. Res., Göttingen,* Rep. UM 6628.

RIABOUCHINSKY, D. 1920 On steady fluid motion with free surfaces. *Proc. Lond. Math. Soc.* **19**, 202.

ROUSE, H. & MCNOWN, J. M. 1948 Cavitation and pressure distribution: headforms at zero angles of yaw. *Bull. St. Univ. Iowa, Studies Engineering,* no. 32.

RUSSELL, D. B. 1963 The numerical solution of problems in fluid flow. Thesis, University of Oxford.

SILVERLEAF, A. 1960 Basic design of the N.P.L. no. 2 water tunnel. *N.P.L. Ship Division, Rep.* no. 15.

SOUTHWELL, R. V. & VAISEY, G. 1946 Fluid motions characterized by free streamlines. *Phil. Trans. Roy. Soc.* **240**, 117.

WAID, R. L. 1957 Water tunnel investigations of two-dimensional cavities. *Calif. Inst. Tech. Rep.* no. E-73.6.

WOODS, L. C. 1951*a* A new relaxation treatment of flow with axial symmetry. *Quart. J. Mech. appl. Math.* **4**, 358.

WOODS, L. C. 1951*b* The relaxation treatment of singular points in Poisson's equation. *Quart. J. Mech. appl. Math.* **6**, 163.

WOODS, L. C. 1961 *The Theory of Subsonic Plane Flow.* Cambridge University Press.

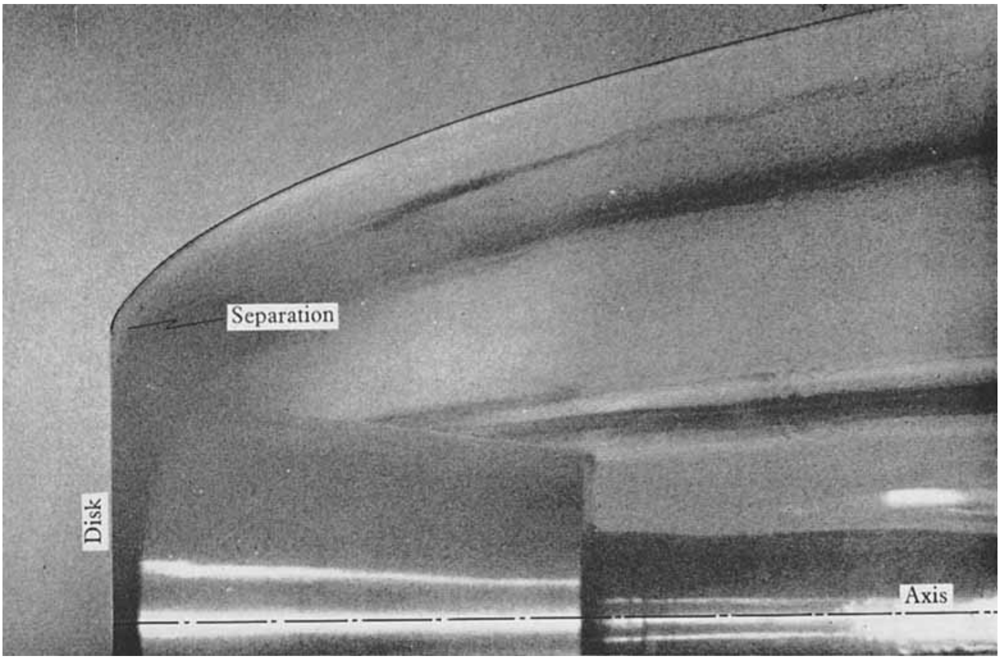

FIGURE 14. Comparison of theoretical and experimental cavity profiles for disk headform ($\sigma = 0{\cdot}2$, $U = 40$ ft./s).

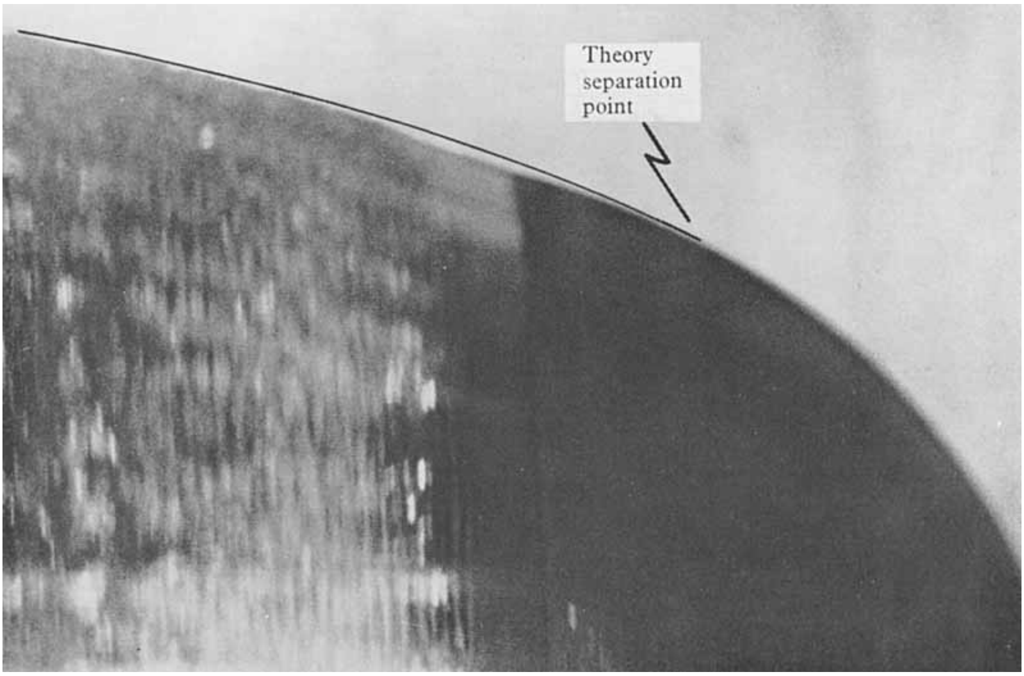

FIGURE 15. Comparison of theoretical and experimental cavity profiles in the region of separation from the sphere ($\sigma = 0{\cdot}2$, $U = 45$ ft./s).